

Demonstration of Hopf-link semimetal bands with superconducting circuits

Xinsheng Tan,¹ Mengmeng Li,¹ Danyu Li,¹ Kunzhe Dai,¹ Haifeng Yu,^{1,*} and Yang Yu^{1,†}

¹*National Laboratory of Solid State Microstructures,
School of Physics, Nanjing University, Nanjing 210093, China*

Hopf-link semimetals exhibit exotic gapless band structures with fascinating topological properties, which have never been observed in nature. Here we demonstrated nodal lines with topological form of Hopf-link chain in artificial semimetal-bands. Driving superconducting quantum circuits with elaborately designed microwave fields, we mapped the momentum space of a lattice to the parameter space, realizing the Hamiltonian of a Hopf-link semimetal. By measuring the energy spectrum, we directly imaged nodal lines in cubic lattices. By tuning the driving fields we adjusted various parameters of Hamiltonian. Important topological features, such as link-unlink topological transition and the robustness of Hopf-link chain structure are investigated. Moreover, we extracted linking number by detecting Berry phase associated with different loops enclosing or disclosing nodal lines. The topological invariant clearly reveals the scenery of the connection between two nodal rings. Our simulations provide foremost knowledge for developing new materials and quantum devices.

As a fundamental mathematics concept, topology plays a very important role in physics research, inspiring many findings in condensed matter physics during past decades. For instance, topological insulators and superconductors[1, 2], which have gapped bulks with topological structures, have been both theoretically and experimentally discovered recently[3–5]. Their topological properties are characterized by nontrivial topological invariants, revealing underlying physics in condensed matter systems. In addition to protected gapped system, gapless band structures also provide fruitful exhibition of topological materials, such as Weyl semimetals[6–10]. The study of band-touching manifolds, including semimetal with 0D nodal points (or Dirac point) and 1D nodal line, deepens our understanding of condensed matter physics [11–13]. Comparing to 0D gapless mode, nodal line provides richer topological structures: nodal rings can touch at special points, resulting various shapes of nodal chains. Recently, it is theoretically predicted that semimetals with a unique nodal chain named Hopf-link structure are possible [11–17]. The Hopf-link, which consists of two rings that pass through the center of each other, represents the simplest topologically nontrivial link. A typical Hamiltonian based on a cubic lattice with Hopf-link structure[18] is given by

$$\begin{aligned} H(\mathbf{k}) &= f_1(\mathbf{k})\sigma_1 + f_2(\mathbf{k})\sigma_3, \\ f_1(\mathbf{k}) &= \sin k_y \cos k_z - \sin k_x \sin k_z, \\ f_2(\mathbf{k}) &= 2\cos k_x + 2\cos k_y + \chi, \end{aligned} \quad (1)$$

where $\sigma_{1,2,3}$ are the Pauli matrices and χ is a tunable parameter. It is easily obtained that nodal lines in the Brillouin zone can be interpreted as the intersecting lines of two surfaces S_x : $f_1(\mathbf{k}) = 0$ and S_y : $f_2(\mathbf{k}) = 0$, forming a novel double-helix structure. Furthermore, due to the periodicity of the Brillouin zone, the cylinder S_y folds into a torus, resulting the double-helix structure deform into a Hopf-chain (as shown in Fig. 1(a)). The nodal loop cannot shrink to a point without crossing each other, leading a finite linking number of the Hopf-chain. This

basic topological invariance can be extracted from Berry phase[19] carried by a closed loop which encircles nodal rings[18, 20]. It is easily to verified that Hamiltonian with Hopf-chain structure obeys PT combined symmetry, while breaking individual symmetry T and P since $[H(\mathbf{k}), PT] = 0$, where T is time reversal operator and P is spatial inversion operator respectively.

In this paper, we have experimentally realized the topological Hopf-link semimetal bands in a square-lattice, via an analogy between the momentum space with a controllable parameter space in superconducting quantum circuits. By measuring the whole energy spectrum of our system in Brillouin zone, we have imaged clearly a gapless band structure of topological semimetals with linked nodal lines. The topological link-unlink phase transitions in semimetal bands can be manipulated by intentionally adding an extra term in the simulated effective Hamiltonian. Furthermore, to demonstrate the topological robustness of the Hopf-link, a perturbation which breaks P and T symmetry while preserves joint PT symmetry is applied. It is verified by experimental data that the Hopf-chain of the topological semimetal bands still present under such perturbations, although the position of nodal lines are changed drastically. To characterize topological properties of Hopf-chain, we extracted the linking numbers of nodal lines by detecting Berry phase after evolving system along designed paths enclosing or disclosing nodal lines respectively[18, 21]. All of these observations illustrate convincingly the topological properties of Hopf-link semimetals, making these systems promising to develop new materials and devices.

The superconducting quantum circuits used in our experiment consist of a superconducting transmon qubit embedded in a three dimensional aluminium cavity [22–25]. The transmon qubit, composed of a single Josephson junction and two pads ($250 \mu\text{m} \times 500 \mu\text{m}$), is patterned using standard e-beam lithography, followed by double-angle evaporation of aluminium on a $500 \mu\text{m}$ thick silicon substrate. The thicknesses of the Al film are 30nm and

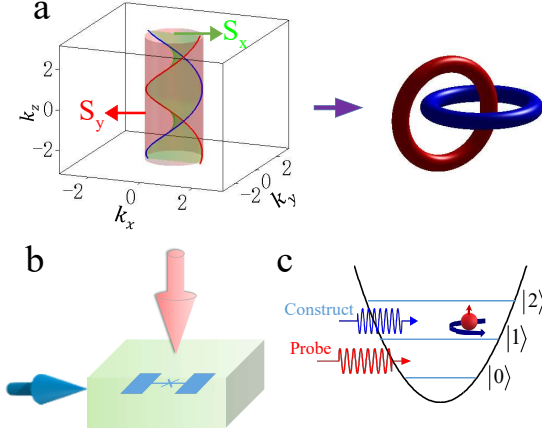


FIG. 1: (Color online) **a**, Nodal lines with a double-Helix structure formed by intersection of two surface S_1 and S_2 . It is topologically equivalent to a Hopf-link. **b**, A superconducting transmon embedded in three-dimensional cavity are driven by designed microwaves, realizing the effective Hamiltonian to simulate Hopf-link semimetal. **c**, The schematic energy structure of a transmon. The lowest three energy levels are used to do simulation.

80nm, respectively. The chip is diced into $3 \text{ mm} \times 6.8 \text{ mm}$ size to fit into the 3D rectangular aluminium cavity with the resonance frequency of TE101 mode 9.053 GHz. The whole sample package is cooled in a dilution refrigerator to a base temperature 10 mK. The transmon can be considered as an artificial atom located in a cavity and the dynamics of the system is generally described by the theory of circuit QED[26–29]. We designed the energy level of the transmon qubit to let the system work in the dispersive region[29]. The quantum states of the transmon qubit can be controlled by microwaves. IQ mixers combined with 1 GHz arbitrary wave generator (AWG) are used to modulate the amplitude, frequency, and phase of microwave pulses. To read out qubit states, we used ordinary microwave heterodyne setup. The output microwave is pre-amplified by HEMT at 4 K stage in the dilution refrigerator and further amplified by two low noise amplifiers in room temperature. The microwave is then heterodyned into 50 MHz and collected by ADCs. The readout is performed with “high power readout” scheme [30]. We sent in a strong microwave on-resonance with the cavity, the transmitted amplitude of the microwave reflects the state of the transmon due to the non-linearity of the cavity QED system.

According to the circuit QED theory, the coupled transmon qubit and cavity exhibit anharmonic multiple energy levels. In our experiments, we used the lowest three energy levels $|0\rangle$, $|1\rangle$, and $|2\rangle$, as shown in Fig. 1c. The two states $|1\rangle$ and $|2\rangle$ behave as an artificial spin-1/2 particle, whose three components may be denoted by the three Pauli matrices $\sigma_{1,2,3}$ which can couple with the microwave fields. $|0\rangle$ is chosen as an ancillary level

to probe the energy spectrum of the simulated system. The transition frequencies between different energy levels are $\omega_{10}/2\pi = 7.172 \text{ GHz}$, $\omega_{21}/2\pi = 6.831 \text{ GHz}$, respectively, which are independently determined by saturation spectroscopies. The energy relaxation time of the qubit is $T_1 \sim 7\mu\text{s}$, the dephasing time is $T_2^* \sim 6\mu\text{s}$. When we apply microwave drive along x , y , and z directions, the effective Hamiltonian of the qubit in the rotating frame may be written as ($\hbar = 1$ for simplicity)

$$\hat{H} = \sum_{i=1}^3 \Omega_i \sigma_i / 2, \quad (2)$$

where Ω_1 (Ω_2) corresponds to the frequency of Rabi oscillations along X (Y) axis on the Bloch sphere, which is continuously adjustable by changing the amplitude and phase of microwave applied to the system. $\Omega_3 = \omega_{21} - \omega_m$, is determined by the detuning between the system energy level spacing ω_{21} and microwave frequency ω_m . By carefully designing the waveform of AWG, we can modulate the frequency, amplitude, and phase of microwave. In our experiment, we first calibrated the parameters Ω_1 , Ω_2 , and Ω_3 using Rabi oscillations and Ramsey fringes, and then designed the microwave amplitude, frequency and phase to set $\Omega_1 = \Omega(\sin k_y \cos k_z - \sin k_x \sin k_z)$, $\Omega_2(k_x) = 0$, $\Omega_3(k_y) = \Omega(2\cos k_x + 2\cos k_y + \chi)$ point by point in the parameter space, with $\Omega = 10 \text{ MHz}$ being the energy unit. By mapping the parameter space of the driving two-level system to the \mathbf{k} -space of a lattice Hamiltonian system, we now have realized Eq. (1) exactly.

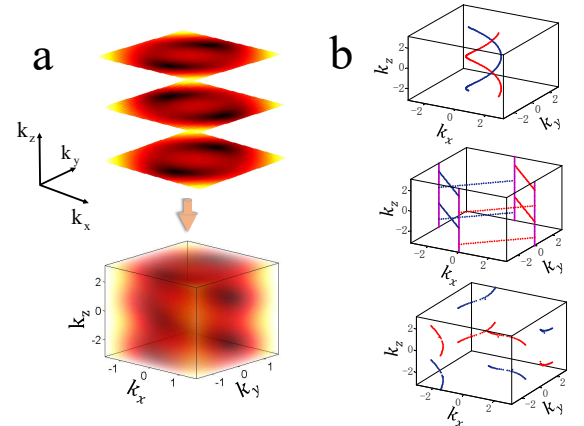


FIG. 2: (Color online) **a**, Measurement of band structure of Hopf-link semimetal in the first Brillouin zone. Top panel: Contour plots of energy gap with varying k_z gradually in the range of $[-\pi, \pi]$. Bottom panel: By collecting all these contour plots together, we obtain the Nodal lines of Hopf-link semimetal. To image gapless band structure clearly, we set the range of (k_x, k_y) as $[-\pi/2, \pi/2] \times [-\pi/2, \pi/2]$. **b**, Nodal lines obtained from measured energy spectrum for various χ . From top to bottom: $\chi = -3, 0$, and 2 , respectively.

It is predicted that χ plays a crucial role in the realization of the double-helix nodal lines in topological semimetal. We first examined the transition of the Hopf-link band structure with the change of χ . Starting from $\chi = -3$, we measured the entire energy spectrum of the system over the first Brillouin zone (BZ). The energy spectrum is measured with spin injection technique [31]. The system is always initialized in $|0\rangle$. For a preset $(k_x, k_y, k_z) \in [-\pi, \pi) \times [-\pi, \pi) \times [-\pi, \pi)$, the construct microwave field drives the two-level system to obtain the Hamiltonian in Eq. (1). A probe microwave pulse is then sent in. When the frequency of probe microwave matches the energy spacing between the eigenenergy of Hamiltonian and $|0\rangle$, the system will be excited to the eigenstate. A resonant peak of microwave absorption can be observed. The frequency of the resonant peak represent the eigenenergy. We then gradually changed k_x, k_y , and k_z , collecting all the eigenenergies from the resonant peaks of the spectrum. We can extract the band structure of semimetal in the first BZ. The zero energy points of the band structure can be directly imaged as nodal points. A chain of connected nodal points forms nodal line. In Fig. 2b, we plot the nodal lines in the first BZ. A feature of the Hopf-link topological semimetal, which is a double-helix structure, is clearly observed, indicating that we have successfully realized the Hopf-link topological semimetal. In addition, the positions of the nodal lines agree well with the theoretical calculation of Eq. (1) with $\lambda = -3$. With the increase of χ , surface S_2 expands, leading double-helix transforms. At $\chi = 0$, S_2 touches the boundary of Brillouin Zone, double-helix deforms to cubic-like shape (middle panel in Fig. 2b). At $\chi = 2$, S_2 opens, forming a cylinder centered at (π, π) . The intersection of S_x and S_y remains double-helix shape (as shown in bottom panel of Fig. 2b).

Furthermore, one can take the advantage of the full tunability of superconducting circuit to demonstrate the topological transition and stability. First we introduce an additional term $H'_1 = \lambda \sin k_y \sigma_1$ to manipulate the topological link-unlink transition. Here H'_1 is in the unit of Ω and λ is an adjustable parameter. Shown in Fig. 3a are nodal-line structure for different λ . When $\lambda < 1$, two nodal lines are linked. As we increased λ to larger than 1, the two nodal lines become separated, forming two topologically unlinked isolation loops. For $\lambda = 1$, the projection of the nodal lines connect at a single point. We can consider this point as the critical point of the transition.

Since the Hamiltonian in Eq. (1) commute with PT , the Hopf-link is protected by the joint space-time symmetry. In order to verify this, we add a term $H'_2 = \eta \sigma_3$ (with η in the unit of Ω) to the Hamiltonian in Eq.1. The modified Hamiltonian violates single P and T symmetry but preserves joint PT symmetry. it is found that with the increase of η , the band structure is distorted dramatically, and the positions as well as neighborhood ge-

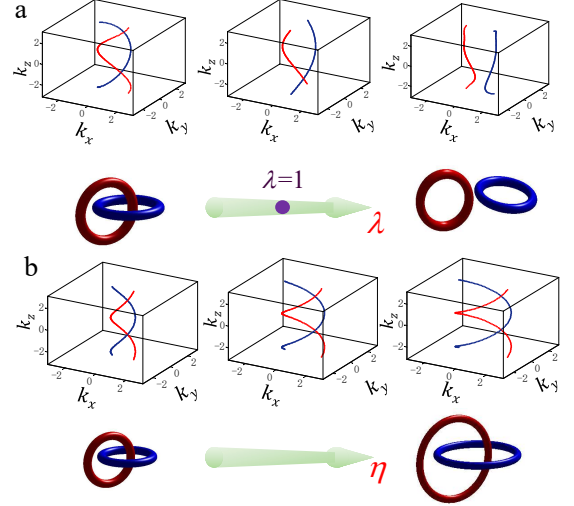


FIG. 3: (Color online) **a**, Link-unlink transition of Hopf-link semimetal after we added $H'_1 = \lambda \sin k_y \sigma_1$ to the Hamiltonian in Eq. 1. From left to right: nodal lines with $\lambda = 0.5, 1$, and 1.5 , respectively. As predicted, $\lambda = 1$ is the critical point, where two nodal rings only touch at one point. **b**, Stability of Hopf-link against the perturbation of $H'_2 = \eta \sigma_3$. From left to right: nodal lines with $\eta = -0.5, 0.5$, and 1.5 , respectively.

ometries of band-crossing lines are changed significantly. Nevertheless, these nodal lines are persistently present in the BZ without opening any gap thus forming double Helix, as shown in Fig. 3b. This strongly support that the Hopf-link structure is protect by PT symmetry.

Besides the band structure, the topological invariant quantity is another feature associated with the topological phenomena. To characterize the linking number of Hopf-link, which describes the connection of nodal lines, we detect the Berry phase carried by a closed path enclosing or disclosing nodal lines in the parameter space from adiabatic procedure[32, 33]. As dashed line showed in Fig. 4a, we design a closed path enclosing Hopf-link chains in Brillouin zone to probe Berry phase. The entire adiabatic evolution consists of two parts. One path marked with purple dashed line which threads the link loop contributes a Berry phase π . The other part marked with grey dashed lines contributes null Berry phase. However, the loop in Fig. 4a are in momentum space. We have to map it from momentum space to parameter space of superconducting qubit, as illustrated in Fig. 4b. Theoretically, evolution path denoted by the purple dashed line is topologically equivalent to a circle along meridian of Bloch sphere. Without loss of generality, we design a geodesic to replace original routine by choosing $\{\Omega_x, \Omega_y, \Omega_z\} = \{\sin \theta \cos \phi + \Lambda_1, \Lambda_2 \sin \phi, \cos \theta \cos \phi + \Lambda_1\}$, where $\theta \in [0, \pi]$ and $\phi \in [0, 2\pi]$ are spherical coordinates. By tuning parameters Λ_1 and Λ_2 , we can implement any closed path in Brillouin zone. To detect accumulated Berry phase after evolving, we used Ramsey fringe inter-

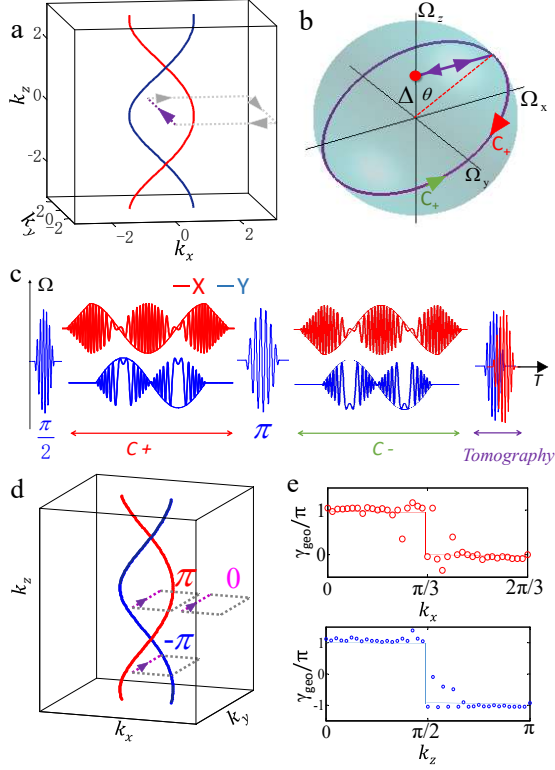


FIG. 4: (Color online) **a**, Schematic of an example of closed path (dashed line) in the first Brillouin zone to accumulate Berry phase, from which the linking number can be characterized. **b**, Evolving path in parameter space of qubit mapped from momentum space in **a**. **c**, Schematic of time profile to probe Berry phase accumulated from the evolution in **b**. **d**, Dependence of the Berry phase carried on the loop of the closed path. There are three typical values: π , $-\pi$, and 0. **e**, Berry phase measured as a function of k_x (top panel) and k_z (down panel), respectively.

ference technique[34, 35]. This adiabatic approach has been demonstrated to be a convenient method to measure the Berry phase in superconducting circuits. If one prepares qubit in a superposition state $(|0\rangle + |1\rangle)/\sqrt{2}$, the evolution of $|0\rangle$ and $|1\rangle$ will acquire a relative Berry phase γ_{geo} , which equals to 1/2 of the solid-angle enclosed by the circle denoted as C_{\pm} . The sign depends on the path direction. The relative phase of the quantum state after the evolution is extracted as $\Phi_{total} = \arctan(\sigma_y/\sigma_x)$, which equals four times of Berry phase. This agrees with the theoretical predict, confirming the topological properties of nodal rings. As shown in Fig. 4d, by adjusting parameters Λ_1 and Λ_2 , we can move the position of closed path in \mathbf{k} -space. By moving the purple dashed line along k_x axis on $k_z = 0$ plane, originally designed closed loop changes from enclosing to disclosing the red nodal line. Geometric phase measured then switch from π to 0 abruptly at $k_x = \pi/3$, indicating closed path in the qubit parameter space is no longer a geodesic circle

at this critical point. Furthermore, by moving the loop along k_z on $k_x = 0$ plane, closed path change from enclosing red nodal line to blue nodal line. The Berry phase jumps from π to $-\pi$ at $k_z = \pi/2$, corresponding Berry phase obtained along C_{\pm} loop. Therefore, in the first Brillouin zone, Berry phase measured are well characterized topological connection of nodal rings.

Experimentally realizing Hopf-link band structures and thus investigating related interesting topological properties in real condensed matter systems are challenge. Nodal lines with Hopf-chain structure has not been observed in any multi-particle system so far. The lack of technique for directly imaging the whole momentum-dependent electronic energy spectrum also prohibits the fundamental research of the complicate topological band structure, noting only a part of electronic spectra (or information of Fermi surfaces/points) may be inferred from the angle-resolved photoemission spectroscopy data (or quantum oscillation measurements) in bulk condensed matter systems. Furthermore, it seems extremely difficult to tune the parameters continuously for studying rich topological properties including various topological quantum phase transitions in real materials. Therefore, our simulations using artificial quantum systems like superconducting quantum circuits provide faithful topological properties of the system, which are useful to design the related materials and devices.

Methods

We used the Ramsey fringe interference technique to measure the Berry phase. The schematic time profile of the measurement procedure is shown in Fig. 4c. At first, qubit is initialized at $(|0\rangle + |1\rangle)/\sqrt{2}$ by a $\pi_y/2$ pulse. Then we ramp the Hamiltonian linearly from $\{0, 0, \Omega_z\}$ to $\{\Omega_x, 0, \Omega_z\}$, followed by traverse along the geodesic path C_+ by ramping parameter $\phi = 2\pi t/T_{ramp}$, where $T_{ramp} = 400$ ns. Since Ω is set as $2\pi \times 25$ MHz, adiabaticity in evolution is satisfied. Instantaneous spin-up and spin-down Eigen-states of Hamiltonian (denoted as $|\uparrow\rangle$ and $|\downarrow\rangle$) has obtained relative phases $\Phi_{c\pm} = \pm\gamma_{geo} + \phi_{dym\uparrow(\downarrow)}$ respectively, where Berry phase $\gamma_{geo} = \pi$ in our experiments and $\phi_{dym\uparrow(\downarrow)}$ is dynamical phase obtained in procedure. After a resonant spin-echo π pulse is applied, system evolves along C_- , which has an opposite direction of C_+ , acquiring $\Phi_{c\mp} = \mp\gamma_{geo} + \phi_{dym\downarrow(\uparrow)}$. The states finally evolve to $\exp[i(\phi_{dym\uparrow} + \phi_{dym\downarrow} + 2\gamma_{geo})]|\uparrow\rangle$ and $\exp[i(\phi_{dym\uparrow} + \phi_{dym\downarrow} - 2\gamma_{geo})]|\downarrow\rangle$, therefore, the neat relative phase gained during complete approach equals $4\gamma_{geo}$ [34]. At the end of the evolution, we extract the phase of qubit state by the quantum state tomography. To map different paths in the first Brillouin zone, Λ_1 and Λ_2 are designed at various values. For instance, to move the closed loop with fixed $k_z = 0$ as shown in Fig. 4d, Λ_1 is varied as $(2\cos k_x - \lambda)/2$ and Λ_2 is set as 1.

Acknowledgements:

We would like to thank Haijun Zhang for helpful suggestion, discussion, and proof reading of the manuscript. This work was partly supported by the the NKRD of China (Grant No. 2016YFA0301802), NSFC (Grant No. 11274156, No. 11504165, No. 11474152, No. 61521001)

* Electronic address: hfyu@nju.edu.cn

† Electronic address: yuyang@nju.edu.cn

- [1] M. Z. Hasan, C. L. Kane, Colloquium: Topological insulators. *Rev. Mod. Phys.* **82**, 3045–3067 (2010).
- [2] X.-L. Qi, S.-C. Zhang, Topological insulators and superconductors. *Rev. Mod. Phys.* **83**, 1057–1110 (2011).
- [3] X. Wan, A. M. Turner, A. Vishwanath, S. Y. Savrasov, Topological semimetal and Fermi-arc surface states in the electronic structure of pyrochlore iridates. *Phys. Rev. B* **83**, 205101 (2011).
- [4] M. König, S. Wiedmann, C. Brune, A. Roth, H. Buhmann, L. W. Molenkamp, X. Qi, S. Zhang, Quantum spin Hall insulator state in HgTe quantum wells. *Science* **318**, 766–770 (2007).
- [5] C. L. Kane, E. J. Mele, Z_2 topological order and the quantum spin Hall effect. *Phys. Rev. Lett.* **95**, 146802 (2005).
- [6] L. Lu, Z. Wang, D. Ye, L. Ran, L. Fu, J. D. Joannopoulos, M. Soljačić, Experimental observation of Weyl points. *Science* **349**, 622–624 (2015).
- [7] S.-Y. Xu, I. Belopolski, N. Alidoust, M. Neupane, G. Bian, C. Zhang, R. Sankar, G. Chang, Z. Yuan, C.-C. Lee, S.-M. Huang, H. Zheng, J. Ma, D. S. Sanchez, B. Wang, A. Bansil, F. Chou, P. P. Shibayev, H. Lin, S. Jia, M. Z. Hasan, Discovery of a Weyl fermion semimetal and topological Fermi arcs. *Science* **349**, 613–617 (2015).
- [8] Z. Liu, J. Jiang, B. Zhou, Z. Wang, Y. Zhang, H. Weng, D. Prabhakaran, S. Mo, H. Peng, P. Dudin, *et al.*, A stable three-dimensional topological Dirac semimetal Cd_3As_2 . *Nature materials* **13**, 677–681 (2014).
- [9] B. Q. Lv, H. M. Weng, B. B. Fu, X. P. Wang, H. Miao, J. Ma, P. Richard, X. C. Huang, L. X. Zhao, G. F. Chen, Z. Fang, X. Dai, T. Qian, H. Ding, Experimental discovery of Weyl semimetal TaAs. *Phys. Rev. X* **5**, 031013 (2015).
- [10] G. Bian, T. Chang, R. Sankar, S. Xu, H. Zheng, T. Neupert, C. Chiu, S. Huang, G. Chang, I. Belopolski, *et al.*, Topological nodal-line fermions in spin-orbit metal PbTaSe_2 . *Nat. Commun.* **7**, 10556–10556 (2016).
- [11] O. Vafek, A. Vishwanath, Dirac fermions in solids: From high-Tc cuprates and graphene to topological insulators and Weyl semimetals. *Annual Review of Condensed Matter Physics* **5**, 83–112 (2014).
- [12] R. Yu, H. Weng, Z. Fang, X. Dai, X. Hu, Topological node-line semimetal and dirac semimetal state in antiperovskite Cu_3PdN . *Phys. Rev. Lett.* **115**, 036807 (2015).
- [13] Y. Kim, B. J. Wieder, C. L. Kane, A. M. Rappe, Dirac line nodes in inversion-symmetric crystals. *Phys. Rev. Lett.* **115**, 036806 (2015).
- [14] A. Burkov, M. D. Hook, L. Balents, Topological nodal semimetals. *Physical Review B* **84** (2011).
- [15] J. E. Moore, Y. Ran, X. Wen, Topological surface states in three-dimensional magnetic insulators. *Phys. Rev. Lett.* **101**, 186805 (2008).
- [16] B.-J. Yang, N. Nagaosa, Classification of stable three-dimensional Dirac semimetals with nontrivial topology. *Nat. Commun.* **5** (2014).
- [17] M. Neupane, S.-Y. Xu, R. Sankar, N. Alidoust, G. Bian, C. Liu, I. Belopolski, T.-R. Chang, H.-T. Jeng, H. Lin, A. Bansil, F. Chou, M. Z. Hasan, Observation of a three-dimensional topological Dirac semimetal phase in high-mobility Cd_3As_2 . *Nat. Commun.* **5**, 3786 (2014).
- [18] W. Chen, H.-Z. Lu, J.-M. Hou, Topological semimetals with a double-helix nodal link. *Phys. Rev. B* **96**, 041102 (2017).
- [19] M. V. Berry, Quantal phase factors accompanying adiabatic changes. *Proceedings of The Royal Society of London* **392**, 45–57 (1984).
- [20] P.-Y. Chang, C.-H. Yee, Weyl-link semimetals. *Phys. Rev. B* **96**, 081114 (2017).
- [21] Z. Yan, R. Bi, H. Shen, L. Lu, S.-C. Zhang, Z. Wang, Nodal-link semimetals. *Phys. Rev. B* **96**, 041103 (2017).
- [22] H. Paik, D. I. Schuster, L. S. Bishop, G. Kirchmair, G. Catelani, A. P. Sears, B. R. Johnson, M. J. Reagor, L. Frunzio, L. I. Glazman, S. M. Girvin, M. H. Devoret, R. J. Schoelkopf, Observation of high coherence in Josephson junction qubits measured in a three-dimensional circuit QED architecture. *Phys. Rev. Lett.* **107**, 240501 (2011).
- [23] M. H. Devoret, R. J. Schoelkopf, Superconducting circuits for quantum information: an outlook. *Science* **339**, 1169–1174 (2013).
- [24] S. Shankar, M. Hatridge, Z. Leghtas, K. Sliwa, A. Narla, U. Vool, S. M. Girvin, L. Frunzio, M. Mirrahimi, M. H. Devoret, Autonomously stabilized entanglement between two superconducting quantum bits. *Nature* **504**, 419–422 (2013).
- [25] C. Wang, Y. Y. Gao, I. M. Pop, U. Vool, C. Axline, T. Brecht, R. W. Heeres, L. Frunzio, M. H. Devoret, G. Catelani, *et al.*, Measurement and control of quasiparticle dynamics in a superconducting qubit. *Nat. Commun.* **5** (2014).
- [26] A. Blais, R.-S. Huang, A. Wallraff, S. M. Girvin, R. J. Schoelkopf, Cavity quantum electrodynamics for superconducting electrical circuits: An architecture for quantum computation. *Phys. Rev. A* **69**, 062320 (2004).
- [27] A. Wallraff, D. I. Schuster, A. Blais, L. Frunzio, R. Huang, J. Majer, S. Kumar, S. M. Girvin, R. J. Schoelkopf, Strong coupling of a single photon to a superconducting qubit using circuit quantum electrodynamics. *Nature* **431**, 162 (2004).
- [28] J. Koch, T. M. Yu, J. Gambetta, A. A. Houck, D. I. Schuster, J. Majer, A. Blais, M. H. Devoret, S. M. Girvin, R. J. Schoelkopf, Charge-insensitive qubit design derived from the Cooper pair box. *Phys. Rev. A* **76**, 042319 (2007).
- [29] J. Q. You, F. Nori, Quantum information processing with superconducting qubits in a microwave field. *Phys. Rev. B* **68**, 064509 (2003).
- [30] M. D. Reed, L. DiCarlo, B. R. Johnson, L. Sun, D. I. Schuster, L. Frunzio, R. J. Schoelkopf, High-fidelity readout in circuit quantum electrodynamics using the Jaynes-Cummings nonlinearity. *Phys. Rev. Lett.* **105**, 173601 (2010).
- [31] X. Tan, Y. Zhao, Q. Liu, G. Xue, H. Yu, Z. D. Wang, Y. Yu, Realizing and manipulating space-time inversion

- symmetric topological semimetal bands with superconducting quantum circuits. *npj Quantum Materials* **2**, 60 (2017).
- [32] D. A. Abanin, T. Kitagawa, I. Bloch, E. Demler, Interferometric approach to measuring band topology in 2D optical lattices. *Phys. Rev. Lett.* **110**, 165304 (2013).
- [33] D. Xiao, M. Chang, Q. Niu, Berry phase effects on electronic properties. *Rev. Mod. Phys.* **82**, 1959–2007 (2010).
- [34] P. J. Leek, J. M. Fink, A. Blais, R. Bianchetti, M. Göppl, J. M. Gambetta, D. I. Schuster, L. Frunzio, R. J. Schoelkopf, A. Wallraff, Observation of Berry’s phase in a solid-state qubit. *Science* **318**, 1889–1892 (2007).
- [35] X. Tan, D.-W. Zhang, Z. Zhang, Y. Yu, S. Han, S.-L. Zhu, Demonstration of geometric Landau-Zener interferometry in a superconducting qubit. *Phys. Rev. Lett.* **112**, 027001 (2014).